Supplement of

Unveiling the Formation of Atmospheric Oxygenated Organic Molecules under Anthropogenic-Biogenic Interactions: Insights from Binned Positive Matrix Factorization on Multi-Subrange Mass Spectra

Junchao Yin & Yuliang Liu et al.
Correspondence to: Wei Nie (niewei@nju.edu.cn)

Table of Contents

S1 Related Calculation of OOMs

Carbon oxidation state (OSc). The OSc of each non-nitro OOM was calculated based on Eq. 1 modified from that in Kroll et al. (2011) include organic nitrate contributions, by assuming that all nitrogen come from the nitrate group (-ONO_2).

$$OS_c = \frac{2(n_O - 3n_N)}{n_C} - \frac{n_H}{n_C} + \frac{n_N}{n_C}. \quad (1)$$

Double bond equivalent (DBE). The DBE of each OOM was calculated using Eq.2, based on the assumption that all nitrogen come from the nitrate group (-ONO_2) or nitro group (-NO_2). DBE represents the combined effect of double or triple bonds, as well as the ring structure in the molecule, helping to identify the class of precursors of OOM (Nie et al., 2022).

$$DBE = n_C + 1 - \frac{n_H + n_N}{2}. \quad (2)$$

Effective Oxygen Number ($n_{O_{eff}}$). The effective oxygen number was calculated using Eq.3, by assuming that all nitrogen of non-nitro OOM come from the nitrate group (-ONO_2):

$$n_{O_{eff}} = n_O - 2 \times n_N. \quad (3)$$

Volatility Basis Set (VBS). The saturation concentration at 300K of OOMs can be used as a characterization of volatility and was calculated using Eq.4 based on the group-contribution method proposed by Donahue et al. (2011):

$$log_{10}C^*(300K) = (25 - n_C) \cdot b_C - (n_O - 2n_N) \cdot b_O - 2b_{CO}\left[\frac{(n_O - 2n_N) \cdot n_C}{n_C + n_O - 2n_N}\right]. \quad (4)$$

where b_C=0.475, b_O=2.3, b_{CO}=-0.3. The effect of nitrate group (-ONO_2) on volatility is similar to hydroxyl group (-OH).

Furthermore, since monoterpene-derived OOMs primarily contain hydroperoxide groups (-OOH) and nitrate groups (-ONO_2), their saturation concentrations were estimated using methods reported by Mohr et al. (2019):

$$log_{10}C^*(300K) = (25 - n_C) \cdot b_C - (n_O - 3n_N) \cdot b_O - 2b_{CO}\left[\frac{(n_O - 3n_N) \cdot n_C}{n_C + n_O - 3n_N}\right] - n_N \cdot b_N. \quad (5)$$

where b_C=0.475, b_O=0.2, b_{CO}=0.9, b_N=2.5. In this study, the identification of monoterpene-related compounds was based on the approach proposed by Nie et al. (2022), where OOMs with DBE=2 that appeared in the PMF monoterpene-related factors were classified as monoterpene OOMs.

The temperature dependence of volatilities is described by Eq.6, according to Stolzenburg et al. (2018):

$$log_{10}C_i^*(T) = log_{10}C_i^*(300K) + \frac{\Delta H_{vap}}{R \cdot \ln(10)}\left(\frac{1}{300} - \frac{1}{T}\right) \quad (6)$$

The evaporation enthalpy (ΔH_{vap}) can be linked to the saturation mass concentration at 300K, $\log_{10}$C*(300K), based on Donahue et al. (2011) and combined with Epstein et al. (2010):

$$\Delta H_{vap}[kJ\ mol^{-1}] = 129 - 5.7 \cdot log_{10}C_i^*(300K) \quad (7)$$

Hydroxyl radical (OH) estimate. The concentration of OH radical was calculated by applying Eq.8, based on the assumption that gaseous SA is produced primarily by the oxidation of SO_2 by OH and is lost mainly through condensation on particles.

$$[OH] = \frac{[H_2SO_4] \cdot CS}{k_{OH+SO_2} \cdot [SO_2]}. \quad (8)$$

where the constant k_{OH+SO_2} is a termolecular reaction constant for the rate-limiting step of the formation pathway of SA in the atmosphere (Finlayson-Pitts and Pitts, 2000). The condensation sink (CS) is the loss rate of SA by condensation of the aerosol surface, which is calculated by the following Eq. 9 (Kulmala et al., 2012):

$$CS = 2\pi D \sum_i \beta_{m_i} d_{p_i} N_i\,. \quad (9)$$

where D is the diffusion coefficient of gaseous SA, β_m is a transition-regime correction factor dependent on the Knudsen number (Fuchs and Sutugin, 1971), and d_{pi} and N_i are the diameter and number concentration of particles in size bin i.

S2 PMF input and diagnostics for each range

S2.1 binPMF inputs

Consistent with previous studies employing the binPMF methodology (Liu et al., 2021, 2023), the mass spectrometry data were divided into narrow bins with a width of 0.004 Th after mass axis calibration to construct the input data matrix for PMF analysis. Data quality control measures were implemented by excluding periods of instrumental instability and retaining only signal regions with meaningful signals in the mass spectra between N-0.1 and N+0.4 Th. The three ranges contained 17280, 18105, 18812 bins. The data were averaged into 30 min time resolution, and finally we got 1679 time points in the data matrix. The error matrix was calculated according to Zhang et al. (2019). To minimize the potential influence of nitrophenols and fluorinated contaminants on the final PMF results, these compounds were systematically down-weighted in the analysis.

S2.2 Diagnosis of binPMF solutions

As established in previous works applying PMF (Ulbrich et al., 2009; Yan et al., 2016), determining the optimal number of factors represents a critical step in the interpretation of PMF results. Accordingly, we systematically evaluated and diagnostically examined solutions encompassing a comprehensive range of factor numbers from 1 to 20 to ensure robust factor resolution. The Q/Q_{exp} ratio exhibited a decreasing trend with increasing factor numbers, albeit with a diminishing rate of reduction (Fig. S1). When the number of PMF factors exceeded eight across all mass ranges, the Q/Q_{exp} ratio stabilized at relatively low levels, accompanied by an explanation ratio exceeding 90% for the original dataset. While higher factor numbers facilitate the resolution of more subtle details within the data, excessive factor decomposition may lead to physically meaningful factors being artificially fragmented into less interpretable ones. In the Range 1, significant influence from nitrophenols was observed. The 10-factor solution successfully isolated and removed the nitrophenol-dominated factors without compromising subsequent analytical interpretations. The N2-MT-I factor was only resolved in the 12-factor solution. Further increasing the number of factors did not yield additional meaningful factors but rather resulted in excessive decomposition of existing factors, thereby compromising the analytical utility of the solution. Consequently, we conducted rotational ambiguity analysis on the 12-factor solution, systematically varying the fpeak parameter from -1 to 1 with an increment of 0.1. Notably, for R1, the fpeak range was extended to 1.5 to identify potentially more optimal solutions. Through this rotational analysis, we selected solutions that maximized the separation between contamination factors and NP-dominated factors. These specifically separated factors were subsequently excluded from further analytical consideration. Similarly, we performed this analytical framework to both R2 and R3, ultimately identifying 11-factor solutions as the optimal configurations for each respective dataset.

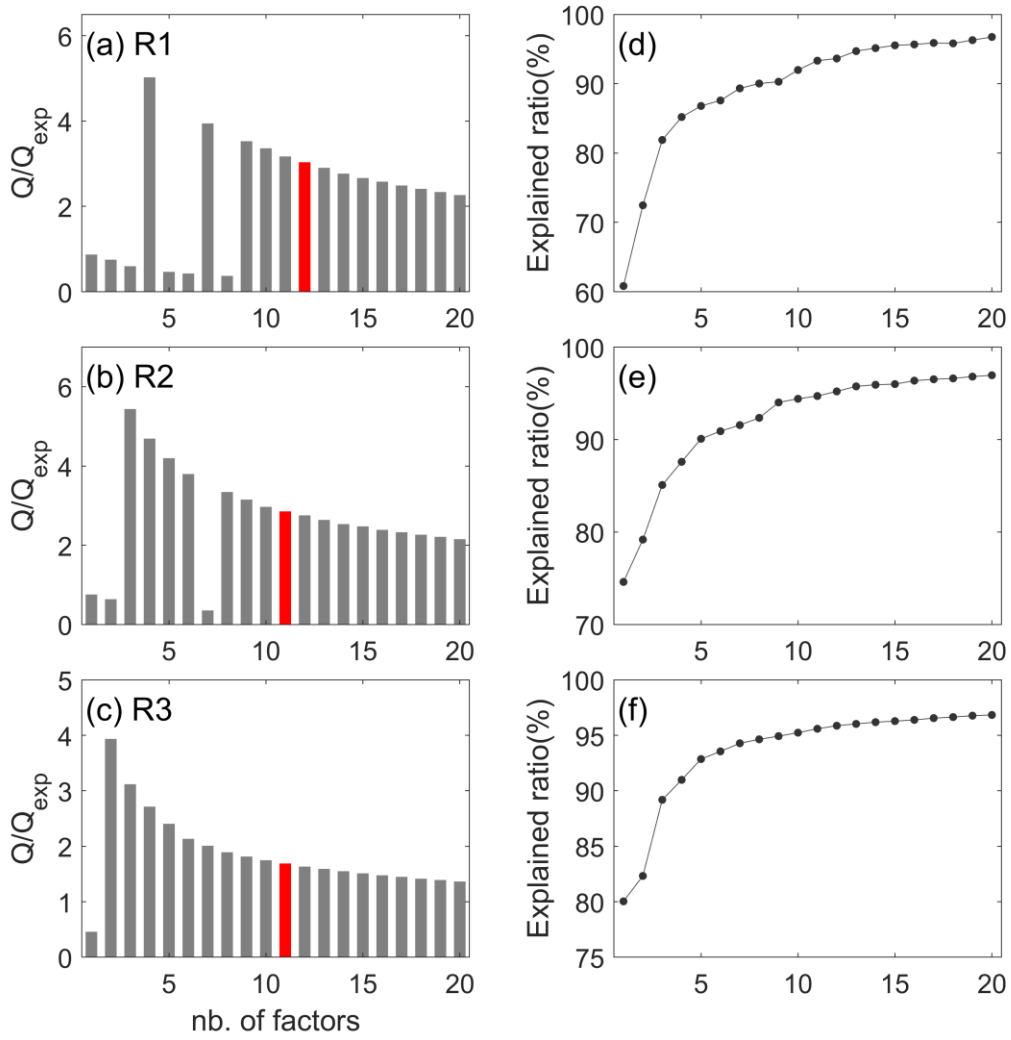

Figure S1. Diagnistics of PMF solutions, including (a)-(c) the variation of Q/Q_{exp} and (d)-(f) explained ratio of PMF factors relative to the number of factors in three range. The red bars indicate the selected PMF solution.

S3 Selected PMF solution for each range

The final PMF solutions selected for each range are presented in Fig. S2-S4. Notably, Range 3 exhibited two closely related factors (D3-AVOC-III-1, D3-AVOC-III-2) that demonstrated strong correlation with corresponding factors in the first two ranges only after factor merging. Therefore, these two factors were consolidated into a single composite factor (D3-AVOC-III) for subsequent analytical interpretation.

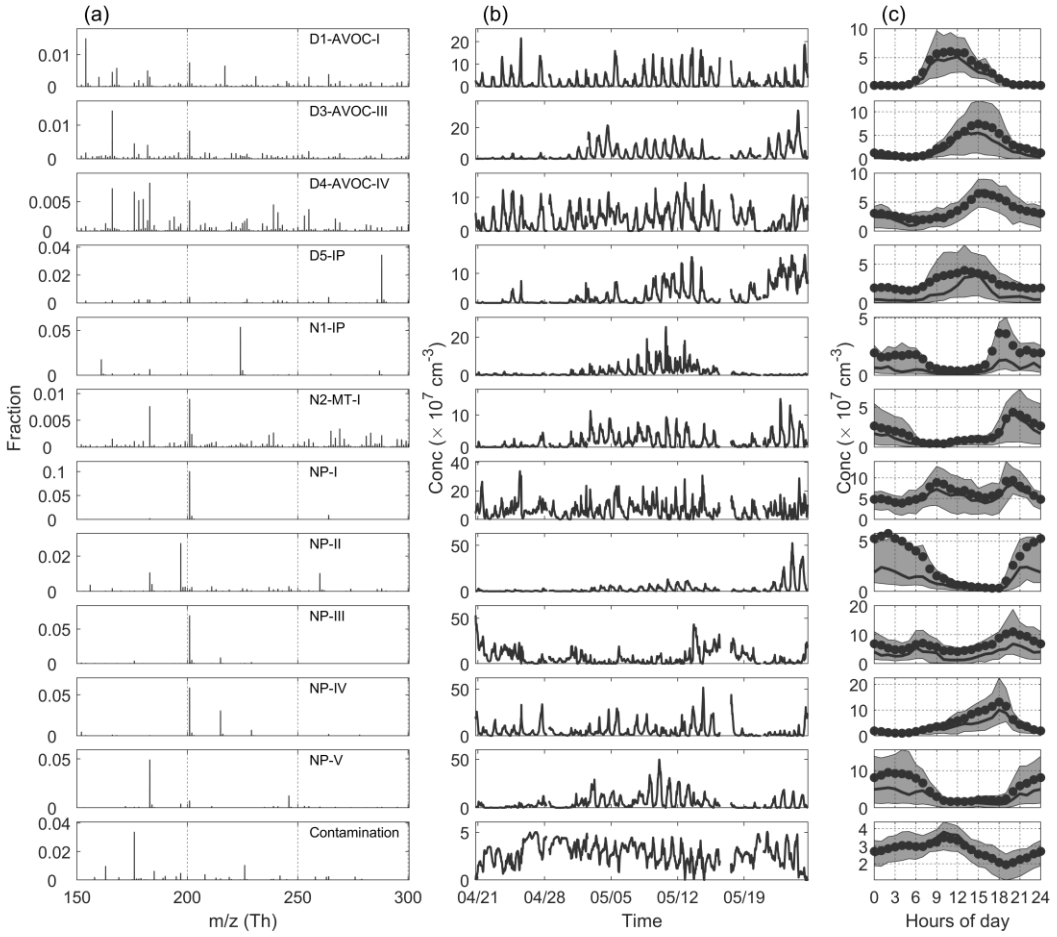

Figure S2. Selected PMF solution for Range 1. (a) PMF factor profiles. (b) Time series of these factors. (c) Diurnal variations in PMF factors.

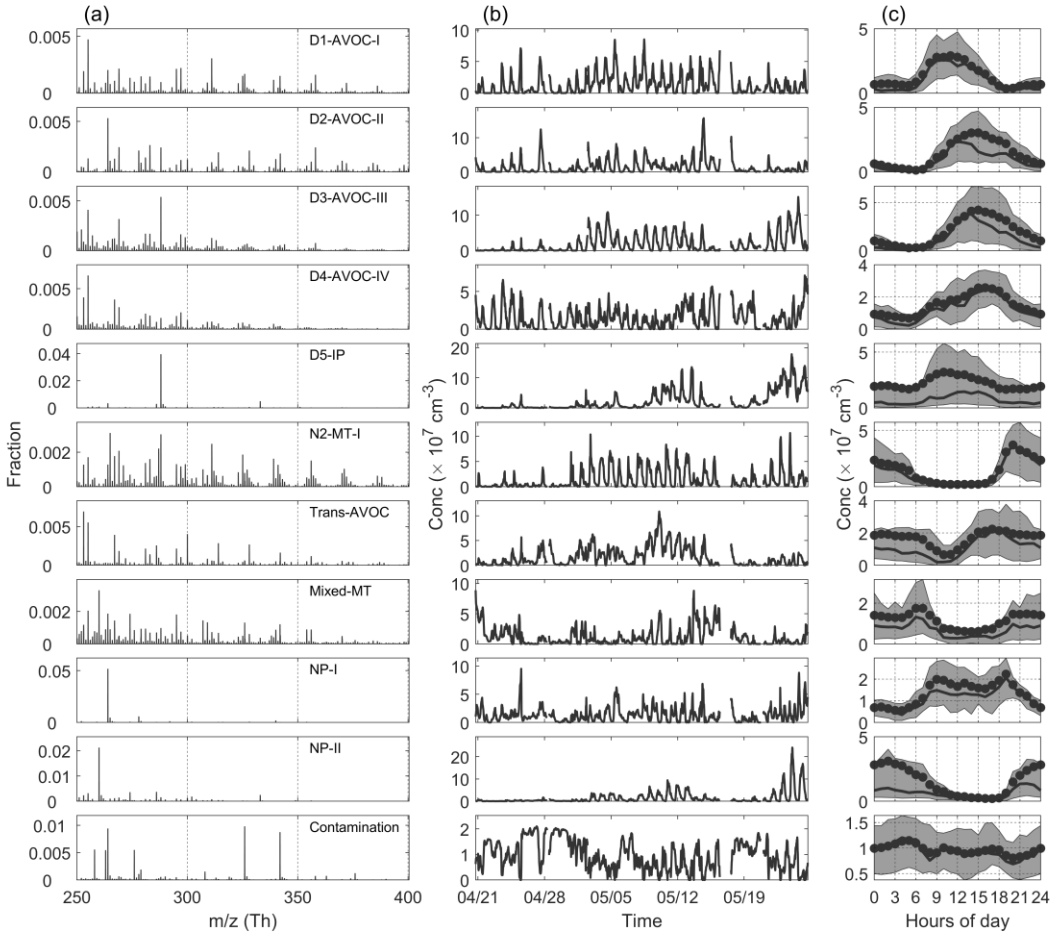

Figure S3. Selected PMF solution for Range 2. (a) PMF factor profiles. (b) Time series of these factors. (c) Diurnal variations in PMF factors.

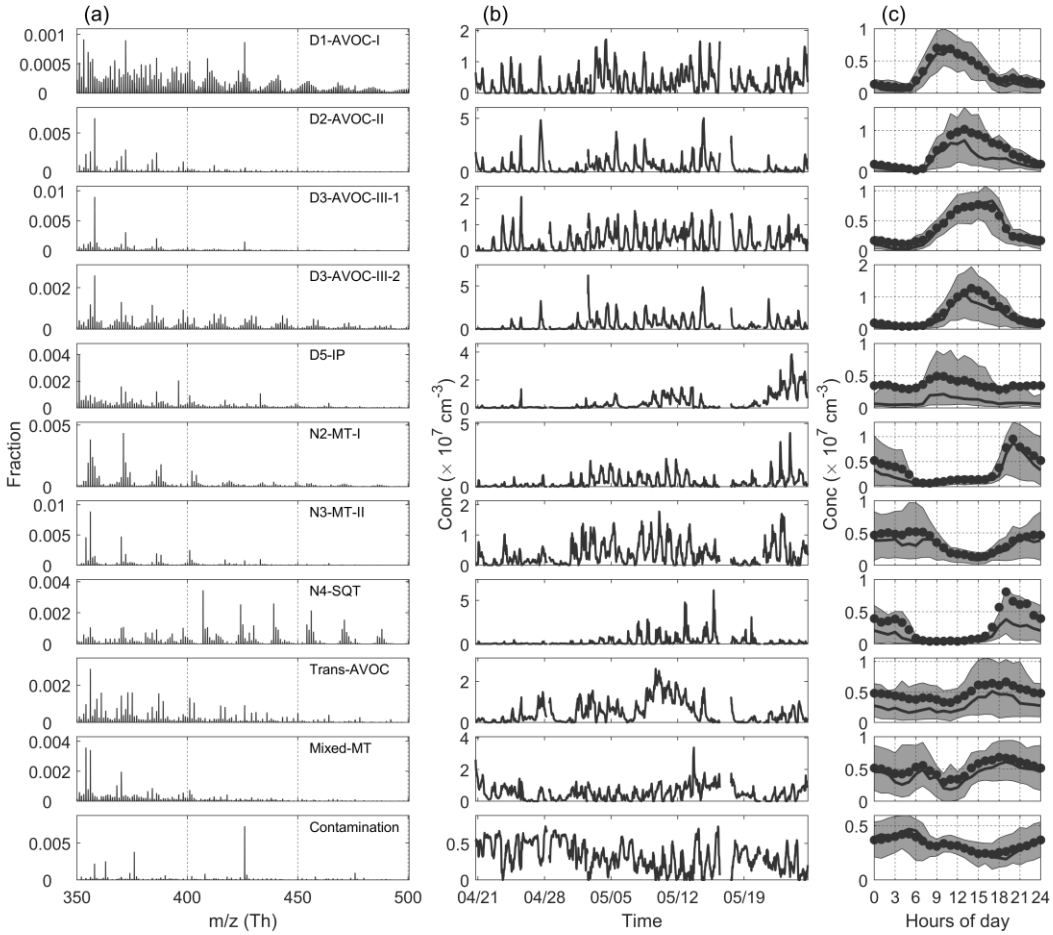

Figure S4. Selected PMF solution for Range 3. (a) PMF factor profiles. (b) Time series of these factors. (c) Diurnal variations in PMF factors.

S4 Correlation of binPMF factors with other data

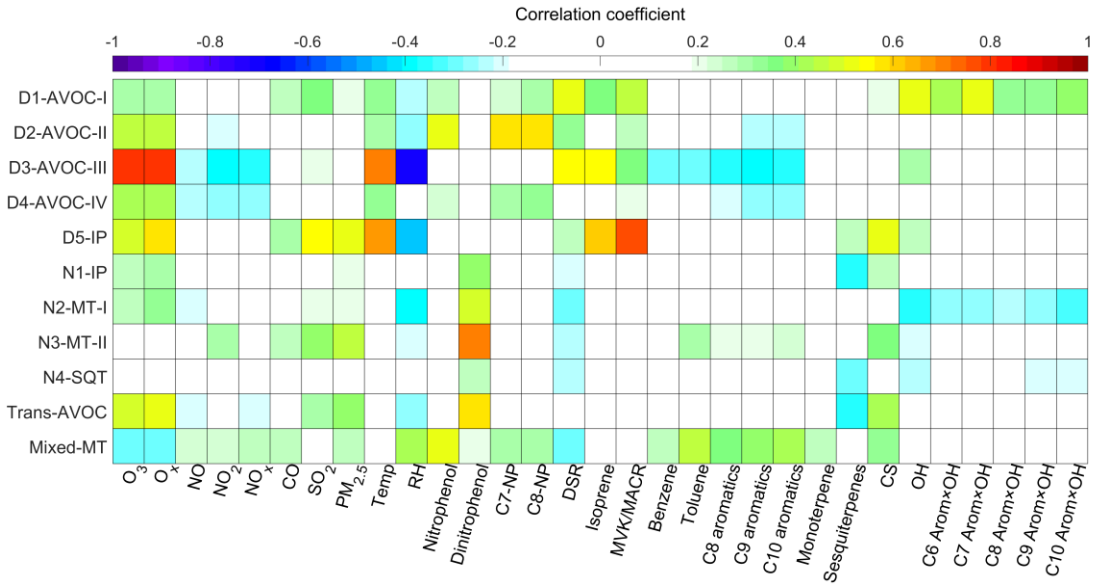

Figure S5. Correlations of factors with external gas-phase and particulate tracers. The colors are differentiated by Pearson correlation coefficients.

S5 Dynamic chemical analysis of specific factors

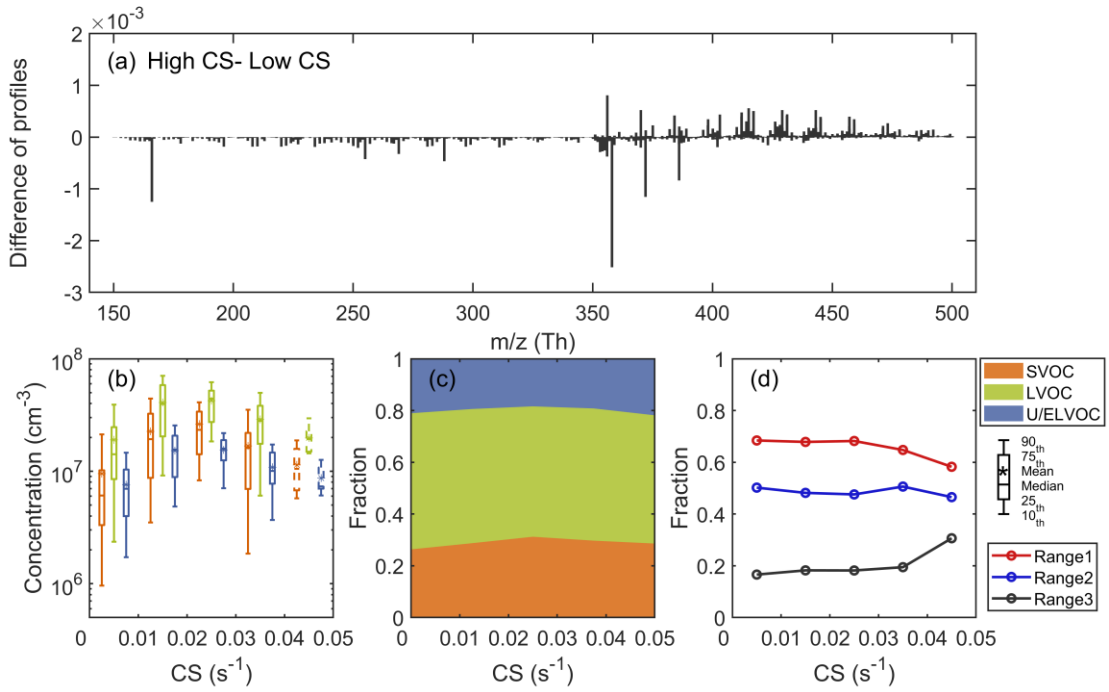

Figure S6. Characteristics of the D3-AVOC-III factor under varying condensation sink (CS) conditions. (a) Difference between the average mass spectra of D3-AVOC-III under high CS (above the upper quartile) and low CS (below the lower quartile) conditions. (b) Boxplots of the concentrations of SVOC, LVOC, and U/ELVOC species binned by CS in each 0.01 s^{-1} interval. Data for CS > 0.04 s^{-1} are represented by dashed box plots owing too few data points. (c) Fractional contributions of SVOC, LVOC, and U/ELVOC species across different CS conditions. (d) Evolution of fractional contributions of three sub-ranges as a function of CS.

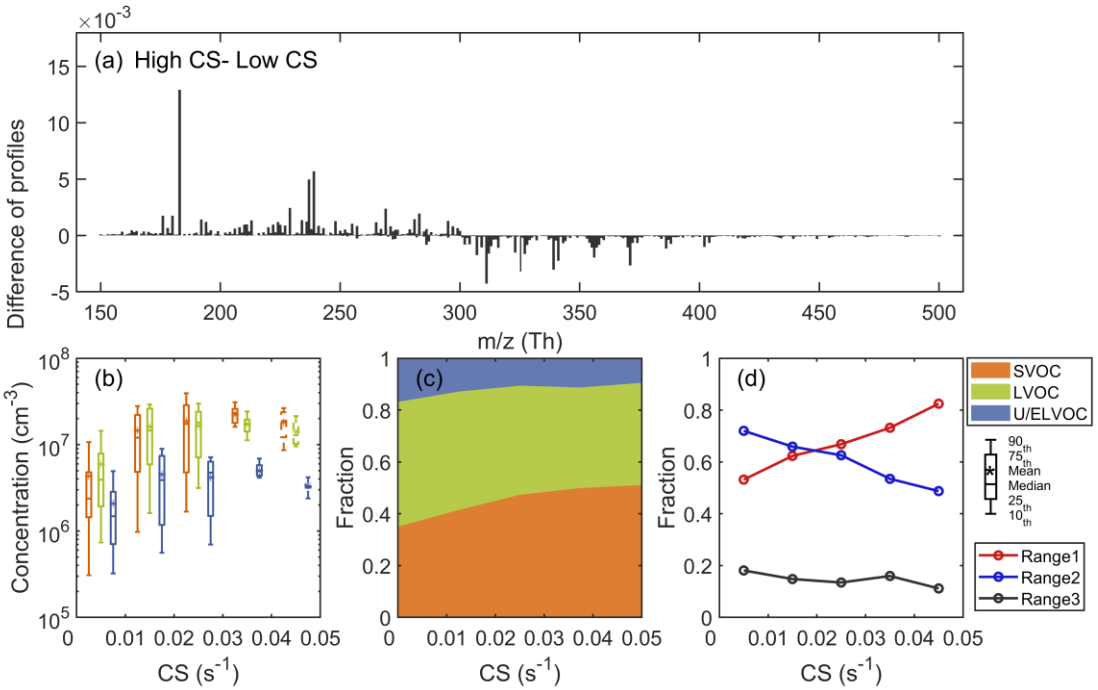

Figure S7. Characteristics of the N2-MT-I factor under varying condensation sink (CS) conditions. (a) Difference between the average mass spectra of N2-MT-I under high CS (above the upper quartile) and low CS (below the lower quartile) conditions. (b) Boxplots of the concentrations of SVOC, LVOC, and U/ELVOC species binned by CS in each 0.01 s^{-1} interval. Data for CS > 0.04 s^{-1} are represented by dashed box plots owing too few data points. (c) Fractional contributions of SVOC, LVOC, and U/ELVOC species across different CS conditions. (d) Evolution of fractional contributions of three sub-ranges as a function of CS.

S6 Main peaks of binPMF factors

Table S1. Molecular characteristics of D1-AVOC-I factor. The reagent ion has been omitted from the formulas.

Range	No.	Formulas	Contribution to the Range (%)	DBE	n_O	n_N
R1	1	$C_xH_{2x-1}O_6N$, x = [3, 9]	18.6	1	6	1
	2	$C_xH_{2x-2}O_4$, x = [3, 10]	9.6	2	4	0
	3	$C_xH_{2x-3}O_7N$, x = [4, 8]	8.3	2	7	1
	4	$C_xH_{2x-3}O_6N$, x = [4, 9]	6.7	2	6	1
	5	$C_xH_{2x-5}O_7N$, x = [5, 8]	5.1	3	7	1
R2	1	$C_xH_{2x-1}O_6N$, x = [6, 13]	13.1	1	6	1
	2	$C_xH_{2x-5}O_8N$, x = [5, 14]	9.9	3	8	1
	3	$C_xH_{2x-3}O_7N$, x = [5, 15]	8.8	2	7	1
	4	$C_xH_{2x-5}O_7N$, x = [5, 14]	7.5	3	7	1
	5	$C_xH_{2x-3}O_6N$, x = [6, 14]	6.1	2	6	1
R3	1	$C_xH_{2x-5}O_8N$, x = [11, 18]	4.3	3	8	1
	2	$C_xH_{2x-5}O_9N$, x = [10, 17]	3.5	3	9	1
	3	$C_xH_{2x-4}O_{10}N_2$, x = [9, 16]	3.3	2	10	2
	4	$C_xH_{2x-3}O_8N$, x = [11, 18]	3.0	2	8	1
	5	$C_xH_{2x-3}O_7N$, x = [12, 18]	2.8	2	7	1

Table S2. Molecular characteristics of D2-AVOC-II factor. The reagent ion has been omitted from the formulas.

Range	No.	Formulas	Contribution to the Range (%)	DBE	n_O	n_N
R2	1	$C_xH_{2x-2}O_8N_2$, x = [6, 13]	14.8	1	8	2
	2	$C_xH_{2x-3}O_7N$, x = [5, 14]	9.3	2	7	1
	3	$C_xH_{2x-1}O_6N$, x = [6, 14]	9.3	1	6	1
	4	$C_xH_{2x-4}O_{10}N_2$, x = [7, 11]	6.7	2	10	2
	5	$C_xH_{2x}O_8N_2$, x = [5, 13]	6.5	0	8	2
R3	1	$C_xH_{2x-4}O_{10}N_2$, x = [8, 12]	18.3	2	10	2
	2	$C_xH_{2x-2}O_8N_2$, x = [10, 18]	12.3	1	8	2
	3	$C_xH_{2x}O_7N_2$, x = [11, 19]	8.5	0	7	2
	4	$C_xH_{2x-4}O_8N_2$, x = [10, 17]	6.2	2	8	2
	5	$C_xH_{2x}O_8N_2$, x = [10, 15]	4.1	0	8	2

Table S3. Molecular characteristics of D3-AVOC-III factor. The reagent ion has been omitted from the formulas.

Range	No.	Formulas	Contribution to the Range (%)	DBE	n_O	n_N
R1	1	$C_xH_{2x-2}O_4$, x = [3]	12.4	2	4	0
	2	$C_xH_{2x-3}O_7N$, x = [4, 8]	7.6	2	7	1
	3	$C_xH_{2x-4}O_5$, x = [4, 10]	7.3	3	5	0
	4	$C_xH_{2x-6}O_5$, x = [5, 10]	6.1	4	5	0
	5	$C_xH_{2x-2}O_5$, x = [4, 9]	6.0	2	5	0
R2	1	$C_xH_{2x-3}O_7N$, x = [5, 11]	11.1	2	7	1
	2	$C_xH_{2x-5}O_7N$, x = [5, 11]	6.1	3	7	1
	3	$C_xH_{2x-5}O_8N$, x = [5, 12]	6.1	3	8	1
	4	$C_xH_{2x-3}O_8N$, x = [5, 11]	6.0	2	8	1
	5	$C_xH_{2x}O_8N_2$, x = [5]	5.7	0	8	2
R3	1	$C_xH_{2x-4}O_{10}N_2$, x = [8, 15]	13.0	2	10	2
	2	$C_xH_{2x-4}O_9N_2$, x = [9, 16]	5.7	2	9	2
	3	$C_xH_{2x-2}O_9N_2$, x = [9, 16]	4.1	1	9	2
	4	$C_xH_{2x-2}O_8N_2$, x = [10, 16]	4.1	1	8	2
	5	$C_xH_{2x-1}O_{10}N_3$, x = [7, 15]	3.4	0	10	3

Table S4. Molecular characteristics of D4-AVOC-IV factor. The reagent ion has been omitted from the formulas.

Range	No.	Formulas	Contribution to the Range (%)	DBE	n_O	n_N
R1	1	$C_xH_{2x-2}O_4$, x = [3, 9]	16.8	2	4	0
	2	$C_xH_{2x-3}O_6N$, x = [4, 9]	15.4	2	6	1
	3	$C_xH_{2x-1}O_6N$, x = [3, 9]	15.2	1	6	1
	4	$C_xH_{2x-1}O_5N$, x = [2, 5]	9.1	1	5	1
	5	$C_xH_{2x-4}O_4$, x = [5, 10]	6.6	3	4	0
R2	1	$C_xH_{2x-1}O_6N$, x = [6, 12]	14.8	1	6	1
	2	$C_xH_{2x-3}O_6N$, x = [6, 14]	13.9	2	6	1
	3	$C_xH_{2x-3}O_7N$, x = [5, 12]	6.5	2	7	1
	4	$C_xH_{2x-2}O_8N_2$, x = [4, 9]	4.8	1	8	2
	5	$C_xH_{2x-5}O_7N$, x = [7, 13]	4.2	3	7	1

Table S5. Molecular characteristics of D5-IP factor. The reagent ion has been omitted from the formulas.

Range	No.	Formulas	Contribution to the Range (%)	DBE	n_C	n_N
R1	1	$C_5H_{10}O_xN_2$, x = [8]	45.7	0	5	2
	2	$C_5H_9O_xN$, x = [4, 9]	4.6	1	5	1
	3	$C_5H_8O_xN_2$, x = [7, 8]	3.8	1	5	2
	4	$C_4H_7O_xN$, x = [5, 6]	3.6	1	4	1
	5	$C_5H_7O_xN$, x = [3, 8]	3.4	2	5	1
R2	1	$C_5H_{10}O_xN_2$, x = [8, 9]	45.4	0	5	2
	2	$C_5H_9O_xN_3$, x = [10, 11]	6.9	0	5	3
	3	$C_5H_8O_xN_2$, x = [8, 9]	4.0	1	5	2
	4	$C_6H_{10}O_xN_2$, x = [8, 9]	1.8	1	6	2
	5	$C_7H_{10}O_xN_2$, x = [8, 10]	1.6	2	7	2
R3	1	$C_{10}H_{16}O_xN_2$, x = [8, 14]	5.6	2	10	2
	2	$C_5H_{10}O_xN_2$, x = [8]	5.6	0	5	2
	3	$C_{10}H_{17}O_xN_3$, x = [10, 14]	4.3	1	10	3
	4	$C_9H_{14}O_xN_2$, x = [9, 14]	3.9	2	9	2
	5	$C_5H_9O_xN_3$, x = [10]	3.1	0	5	3

Table S6. Molecular characteristics of N1-IP factor. The reagent ion has been omitted from the formulas.

Range	No.	Formulas	Contribution to the Range (%)	DBE	n_C	n_N
R3	1	$C_5H_8O_xN\cdot$, x = [5]	57.4	1.5	5	1
	2	$C_6H_{10}O_x$, x = [5]	8.7	2	6	0
	3	$C_6H_{11}O_xN$, x = [6, 8]	3.8	1	6	1
	4	$C_5H_9O_xN$, x = [5, 6]	2.9	1	5	1
	5	$C_7H_9O_xN$, x = [6, 8]	2.6	3	7	1

Table S7. Molecular characteristics of N2-MT-I factor. The reagent ion has been omitted from the formulas.

Range	No.	Formulas	Contribution to the Range (%)	DBE	n_C	n_N
R1	1	$C_7H_9O_xN$, x = [6, 8]	8.5	3	7	1
	2	$C_2H_3O_xN$, x = [5]	7.0	1	2	1
	3	$C_7H_{11}O_xN$, x = [6, 8]	6.8	2	7	1
	4	$C_6H_9O_xN$, x = [5, 8]	6.4	2	6	1
	5	$C_5H_7O_xN$, x = [5, 8]	5.1	2	5	1
R2	1	$C_7H_9O_xN$, x = [6, 9]	6.7	3	7	1
	2	$C_{10}H_{15}O_xN$, x = [6, 10]	6.6	3	10	1
	3	$C_9H_{15}O_xN$, x = [6, 9]	6.2	2	9	1
	4	$C_{10}H_{17}O_xN$, x = [6, 10]	5.5	2	10	1
	5	$C_6H_{11}O_xN$, x = [6, 9]	5.1	1	6	1
R3	1	$C_{10}H_{15}O_xN$, x = [9, 12]	9.0	3	10	1
	2	$C_{10}H_{16}O_xN_2$, x = [8, 13]	6.3	2	10	2
	3	$C_{10}H_{16}O_xN\cdot$, x = [9, 11]	6.1	2.5	10	1
	4	$C_{10}H_{18}O_xN_2$, x = [8, 12]	5.1	1	10	2
	5	$C_9H_{16}O_xN_2$, x = [9, 13]	4.0	1	9	2

Table S8. Molecular characteristics of N3-MT-II factor. The reagent ion has been omitted from the formulas.

Range	No.	Formulas	Contribution to the Range (%)	DBE	n_C	n_N
R3	1	$C_{10}H_{16}O_xN_2$, x = [8, 13]	17.7	2	10	2
	2	$C_{10}H_{18}O_xN_2$, x = [8, 13]	16.7	1	10	2
	3	$C_{10}H_{17}O_xN_3$, x = [10, 13]	7.4	1	10	3
	4	$C_{10}H_{16}O_xN\cdot$, x = [9, 11]	3.0	2.5	10	1
	5	$C_9H_{16}O_xN_2$, x = [9, 13]	2.9	1	9	2

Table S9. Molecular characteristics of N4-SQT factor. The reagent ion has been omitted from the formulas.

Range	No.	Formulas	Contribution to the Range (%)	DBE	n_C	n_N
R3	1	$C_{15}H_{23}O_xN$, x = [6, 12]	14.3	4	15	1
	2	$C_{15}H_{24}O_xN\cdot$, x = [7, 13]	7.6	3.5	15	1
	3	$C_{15}H_{25}O_xN$, x = [6, 13]	5.8	3	15	1
	4	$C_{15}H_{24}O_xN_2$, x = [8, 12]	5.3	3	15	2
	5	$C_{11}H_{16}O_xN_2$, x = [9, 13]	3.9	3	11	2

Table S10. Molecular characteristics of Trans-AVOC factor. The reagent ion has been omitted from the formulas.

Range	No.	Formulas	Contribution to the Range (%)	DBE	n_O	n_N
R2	1	$C_xH_{2x-2}O_8N_2$, x = [4, 12]	20.2	1	8	2
	2	$C_xH_{2x-3}O_6N$, x = [6, 11]	18.0	2	6	1
	3	$C_xH_{2x-1}O_6N$, x = [6, 10]	10.4	1	6	1
	4	$C_xH_{2x-3}O_{10}N$, x = [5, 11]	5.6	2	10	1
	5	$C_xH_{2x}O_7N_2$, x = [5, 11]	4.5	0	7	2
R3	1	$C_xH_{2x-3}O_{10}N_3$, x = [7, 14]	11.0	1	10	3
	2	$C_xH_{2x-1}O_{10}N_3$, x = [7, 13]	8.0	0	10	3
	3	$C_xH_{2x-3}O_{11}N_3$, x = [6, 14]	7.6	1	11	3
	4	$C_xH_{2x-2}O_8N_2$, x = [10, 14]	7.2	1	8	2
	5	$C_xH_{2x-4}O_9N_2$, x = [9, 14]	5.2	2	9	2

Table S11. Molecular characteristics of Mixed-MT factor. The reagent ion has been omitted from the formulas.

Range	No.	Formulas	Contribution to the Range (%)	DBE	n_O	n_N
R2	1	$C_xH_{2x-3}O_6N$, x = [6, 14]	10.2	2	6	1
	2	$C_xH_{2x-5}O_6N$, x = [6, 15]	7.2	3	6	1
	3	$C_xH_{2x-1}O_6N$, x = [6, 12]	6.6	1	6	1
	4	$C_xH_{2x}O_7N_2$, x = [5, 14]	6.0	0	7	2
	5	$C_xH_{2x-1}O_5N$, x = [7, 13]	5.0	1	5	1
R3	1	$C_xH_{2x-2}O_8N_2$, x = [10, 15]	9.3	1	8	2
	2	$C_xH_{2x-4}O_8N_2$, x = [10, 15]	7.9	2	8	2
	3	$C_xH_{2x-4}O_9N_2$, x = [9, 15]	5.9	2	9	2
	4	$C_xH_{2x}O_7N_2$, x = [11, 16]	5.4	0	7	2
	5	$C_xH_{2x-3}O_{10}N_3$, x = [7, 13]	3.2	1	10	3

Reference:

Donahue, N. M., Epstein, S. A., Pandis, S. N., and Robinson, A. L.: A two-dimensional volatility basis set: 1. organic-aerosol mixing thermodynamics, Atmos Chem Phys, 2011.

Epstein, S. A., Riipinen, I., and Donahue, N. M.: A Semiempirical Correlation between Enthalpy of Vaporization and Saturation Concentration for Organic Aerosol, Environ. Sci. Technol., 44, 743–748, https://doi.org/10.1021/es902497z, 2010.

Finlayson-Pitts, B. J. and Pitts, J. N.: Acid Deposition Formation and Fates of Inorganic and Organic Acids in the Troposphere, in: Chemistry of the Upper and Lower Atmosphere, vol. 8, Academic Press, 294–348, 2000.

Fuchs, N. A. and Sutugin, A. G.: HIGH-DISPERSED AEROSOLS, in: Topics in Current Aerosol Research, Elsevier, 1, https://doi.org/10.1016/B978-0-08-016674-2.50007-8, 1971.

Kroll, J. H., Donahue, N. M., Jimenez, J. L., Kessler, S. H., Canagaratna, M. R., Wilson, K. R., Altieri, K. E., Mazzoleni, L. R., Wozniak, A. S., Bluhm, H., Mysak, E. R., Smith, J. D., Kolb, C. E., and Worsnop, D. R.: Carbon oxidation state as a metric for describing the chemistry of atmospheric organic aerosol, Nat. Chem., 3, 133–139, https://doi.org/10.1038/nchem.948, 2011.

Kulmala, M., Petäjä, T., Nieminen, T., Sipilä, M., Manninen, H. E., Lehtipalo, K., Dal Maso, M., Aalto, P. P., Junninen, H., Paasonen, P., Riipinen, I., Lehtinen, K. E. J., Laaksonen, A., and Kerminen, V.-M.: Measurement of the nucleation of atmospheric aerosol particles, Nat. Protoc., 7, 1651–1667, https://doi.org/10.1038/nprot.2012.091, 2012.

Liu, Y., Nie, W., Li, Y., Ge, D., Liu, C., Xu, Z., Chen, L., Wang, T., Wang, L., Sun, P., Qi, X., Wang, J., Xu, Z., Yuan, J., Yan, C., Zhang, Y., Huang, D., Wang, Z., Donahue, N. M., Worsnop, D., Chi, X., Ehn, M., and Ding, A.: Formation of condensable organic vapors from anthropogenic and biogenic volatile organic compounds (VOCs) is strongly perturbed by NOx in eastern China, Atmospheric Chem. Phys., 21, 14789–14814, https://doi.org/10.5194/acp-21-14789-2021, 2021.

Liu, Y., Liu, C., Nie, W., Li, Y., Ge, D., Chen, L., Zhu, C., Wang, L., Zhang, Y., Liu, T., Qi, X., Wang, J., Huang, D., Wang, Z., Yan, C., Chi, X., and Ding, A.: Exploring condensable organic vapors and their co-occurrence with $PM_{2.5}$ and O_3 in winter in Eastern China, Environ. Sci. Atmospheres, 3, 282–297, https://doi.org/10.1039/D2EA00143H, 2023.

Mohr, C., Thornton, J. A., Heitto, A., Lopez-Hilfiker, F. D., Lutz, A., Riipinen, I., Hong, J., Donahue, N. M., Hallquist, M., Petäjä, T., Kulmala, M., and Yli-Juuti, T.: Molecular identification of organic vapors driving atmospheric nanoparticle growth, Nat. Commun., 10, 4442, https://doi.org/10.1038/s41467-019-12473-2, 2019.

Nie, W., Yan, C., Huang, D. D., Wang, Z., Liu, Y., Qiao, X., Guo, Y., Tian, L., Zheng, P., Xu, Z., Li, Y., Xu, Z., Qi, X., Sun, P., Wang, J., Zheng, F., Li, X., Yin, R., Dallenbach, K. R., Bianchi, F., Petäjä, T., Zhang, Y., Wang, M., Schervish, M., Wang, S., Qiao, L., Wang, Q., Zhou, M., Wang, H., Yu, C., Yao, D., Guo, H., Ye, P., Lee, S., Li, Y. J., Liu, Y., Chi, X., Kerminen, V.-M., Ehn, M., Donahue, N. M., Wang, T., Huang, C., Kulmala, M., Worsnop, D., Jiang, J., and Ding, A.: Secondary organic aerosol formed by condensing anthropogenic vapours over China's megacities, Nat. Geosci., 15, 255–261, https://doi.org/10.1038/s41561-022-00922-5, 2022.

Stolzenburg, D., Fischer, L., Vogel, A. L., Heinritzi, M., Schervish, M., Simon, M., Wagner, A. C., Dada, L., Ahonen, L. R., Amorim, A., Baccarini, A., Bauer, P. S., Baumgartner, B., Bergen, A., Bianchi, F., Breitenlechner, M., Brilke, S., Buenrostro Mazon, S., Chen, D., Dias, A., Draper, D. C., Duplissy, J., El Haddad, I., Finkenzeller, H., Frege, C., Fuchs, C., Garmash, O., Gordon, H., He, X., Helm, J., Hofbauer, V., Hoyle, C. R., Kim, C., Kirkby, J., Kontkanen, J., Kürten, A., Lampilahti, J., Lawler, M., Lehtipalo, K., Leiminger, M., Mai, H., Mathot, S., Mentler, B., Molteni, U., Nie, W., Nieminen, T., Nowak, J. B., Ojdanic, A., Onnela, A., Passananti, M., Petäjä, T., Quéléver, L. L. J., Rissanen, M. P., Sarnela, N., Schallhart, S., Tauber, C., Tomé, A., Wagner, R., Wang, M., Weitz, L., Wimmer, D., Xiao, M., Yan, C., Ye, P., Zha, Q., Baltensperger, U., Curtius, J., Dommen, J., Flagan, R. C., Kulmala, M., Smith, J. N., Worsnop, D. R., Hansel, A., Donahue, N. M., and Winkler, P. M.: Rapid growth of organic aerosol nanoparticles over a wide tropospheric temperature range, Proc. Natl. Acad. Sci., 115, 9122–9127, https://doi.org/10.1073/pnas.1807604115, 2018.

Ulbrich, I. M., Canagaratna, M. R., Zhang, Q., Worsnop, D. R., and Jimenez, J. L.: Interpretation of organic components from Positive Matrix Factorization of aerosol mass spectrometric data, Atmos Chem Phys, 2009.

Yan, C., Nie, W., Äijälä, M., Rissanen, M. P., Canagaratna, M. R., Massoli, P., Junninen, H., Jokinen, T., Sarnela, N., Häme, S. A. K., Schobesberger, S., Canonaco, F., Yao, L., Prévôt, A. S. H., Petäjä, T., Kulmala, M., Sipilä, M., Worsnop, D. R., and Ehn, M.: Source characterization of highly oxidized multifunctional compounds in a boreal forest environment using positive matrix factorization, Atmospheric Chem. Phys., 16, 12715–12731, https://doi.org/10.5194/acp-16-12715-2016, 2016.

Zhang, Y., Peräkylä, O., Yan, C., Heikkinen, L., Äijälä, M., Daellenbach, K. R., Zha, Q., Riva, M., Garmash, O., Junninen, H., Paatero, P., Worsnop, D., and Ehn, M.: A novel approach for simple statistical analysis of high-resolution mass spectra, Atmospheric Meas. Tech., 12, 3761–3776, https://doi.org/10.5194/amt-12-3761-2019, 2019.